Epitaxial metastable $Ge_{1-y}C_y$ ($y \leqslant 0.02$) alloys grown on Ge(001) from hyperthermal beams: C incorporation and lattice sites

J. D'Arcy-Gall,[a] P. Desjardins, I. Petrov, and J. E. Greene
Materials Science Department, the Coordinated Science Laboratory, and the Materials Research Laboratory, University of Illinois, 104 South Goodwin Avenue, Urbana, Illinois 61801

J.-E. Paultre and R. A. Masut
Groupe de Recherche en Physique et Technologie des Couches Minces and Département de Génie Physique et de Génie des Matériaux, Ecole Polytechnique de Montréal, P.O. Box 6079, Station Centre-Ville, Montréal, Québec H3C 3A7, Canada

S. C. Gujrathi and S. Roorda
Groupe de Recherche en Physique et Technologie des Couches Minces and Département de Physique, Université de Montréal, P.O. Box 6128, Station Centre-Ville, Montréal, Québec H3C 3J7, Canada

(Received 4 November 1999; accepted for publication 29 March 2000)

Epitaxial metastable $Ge_{1-y}C_y$ alloy layers with $y \leqslant 0.02$ were grown on Ge(001) at temperatures $T_s = 200-550\,^{\circ}C$ using hyperthermal Ge and C beams with average energies of 16 and 24 eV, respectively, in order to investigate C incorporation pathways in the Ge lattice. High-resolution reciprocal lattice maps show that all as-deposited alloy layers are fully coherent with the substrate. Layers grown at $T_s \leqslant 350\,^{\circ}C$ are in compression due to higher C concentrations in interstitial than in substitutional sites. The compressive strain decreases (i.e., the substitutional C concentration increases) with increasing T_s within this temperature range. At higher growth temperatures, as-deposited alloys are nearly strain free since the majority of the incorporated C is trapped at extended defects. Annealing the $Ge_{1-y}C_y$ layers at $T_a = 450$ and $550\,^{\circ}C$ leads to a significant increase, proportional to the strain in the as-deposited films, in compressive strain. Further annealing at $T_a = 650\,^{\circ}C$ results in the formation of dislocation loops which act as sinks for interstitial and substitutional C atoms and thus relieves residual macroscopic strain. Finally, we show that the large compressive strain associated with interstitial C atoms must be accounted for in order to determine the total incorporated C fraction from diffraction analyses. © *2000 American Institute of Physics.* [S0021-8979(00)03513-1]

I. INTRODUCTION

C-containing group-IV semiconductor alloys are of intense technological and scientific interest due to the potential they offer for both band gap and strain-state engineering of layers used in microelectronic and optoelectronic devices compatible with Si integrated circuit technology. Soref used virtual-crystal linear extrapolations of the Γ, Δ, and L point energies as a function of composition to predict that unstrained $Si_{1-x-y}Ge_xC_y$ alloys should have indirect band gap energies tunable from 0.62 to 5.5 eV.[1] Adding C to $Si_{1-x}Ge_x$ alloy layers pseudomorphically grown on Si(001) rapidly reduces the compressive strain and leads to increased critical thicknesses for the introduction of misfit dislocations. Furthermore, the addition of C to $Si_{1-x}Ge_x$ has been shown to inhibit B diffusion in *npn* bipolar heterojunction transistors,[2] while pseudomorphic $Si_{1-y}C_y/Si(001)$ structures provide sufficient conduction band offset to obtain well-defined two-dimensional electron gases.[3]

There are, however, severe challenges associated with the growth of C-containing group-IV alloys. First, the equilibrium solubility of C in Si and Ge is limited to $\simeq 10^{17}$ and 10^8 cm^{-3}, respectively.[4] This argues for low temperature growth under highly kinetically constrained conditions to take advantage of the fact that surface solubilities are orders of magnitude larger than bulk values,[5] while simultaneously inhibiting phase separation during deposition. Another obstacle to be overcome is the extremely large lattice constant mismatch between diamond ($a_C = 3.5668$ Å) and the common group-IV semiconductors Si ($a_{Si} = 5.4310$ Å) and Ge($a_{Ge} = 5.6576$ Å). Moreover, C atoms, due to their very small covalent radii, tend to incorporate on nonsubstitutional lattice sites in Si and $Si_{1-x}Ge_x$ and/or to form defect complexes. The general trend observed during solid-source molecular beam epitaxy (MBE) and chemical vapor deposition (CVD) of $Si_{1-y}C_y/Si(001)$ and $Si_{1-x-y}Ge_xC_y/Si(001)$ is that substitutional C incorporation increases with decreasing growth temperature T_s and increasing growth rates.[6] Complete incorporation of C atoms into substitutional sites in $Si_{1-x}C_x$ and $Ge_{1-y}C_y$ alloys has been achieved only for low C concentrations and a very narrow window of growth conditions. The maximum reported substitutional C concentration, irrespective of the total C content, is 2.7 at.% in $Si_{0.526}Ge_{0.43}C_{0.044}/Si$ superlattice structures grown on Si(001) by MBE at $T_s = 500-600\,^{\circ}C$.[7] The $y = 0.027$ value, however, was obtained from x-ray diffraction data without accounting for the strain induced by the nonsubstitutional C

[a]Author to whom correspondence should be addressed; electronic mail: darcy@uiuc.edu

and, hence, is probably incorrect, as discussed below.

In order to reduce the in-plane compressive strain and to controllably tailor the optoelectronic properties of $Si_{1-x-y}Ge_xC_y$ alloys grown on Si, C must be incorporated into substitutional sites. However, essentially nothing is known about detailed C incorporation mechanisms and pathways in $Si_{1-x-y}Ge_xC_y$ during epitaxial growth. The substitutional site is the most energetically favorable one for C incorporation in bulk Si,[8] but C is simultaneously incorporated into interstitial sites during $Si_{1-y}C_y$ film growth. The most stable interstitial configuration for C in Si is a C–Si split interstitial on a single substitutional lattice site.[9] However, C in this configuration has an energy which is 3 eV higher than C on a substitutional site.[8] Local-orbital quantum molecular-dynamics calculations of the C-induced tetragonal strain in $Si_{1-x}C_x/Si(001)$ and $Si_{1-x-y}Ge_xC_y/Si(001)$ alloys[9] show that complete C incorporation into substitutional sites leads to the maximum possible tensile strain while films in compression are obtained when C is incorporated as Si–C split interstitials.

According to Windl *et al.*,[9] the tensile strain induced by substitutional C incorporation is almost a factor of two larger than predicted by Vegard's rule, yielding a strain compensation ratio, defined as the ratio of Ge to C atomic fractions in Si required to maintain the lattice constant of Si, of $\simeq 15$.[9] The calculations of Windl *et al.* also clearly demonstrate that the strain induced by interstitial C is not negligible and may even be comparable to the strain of substitutional C. Therefore, reported substitutional concentrations in $Si_{1-x}C_x$ and $Ge_{1-y}C_y$ layers, which are typically estimated from XRD results alone, are incorrect.

C incorporation into $Ge_{1-y}C_y$ alloys has received less attention than in $Si_{1-y}C_y$ alloys. Hoffman and co-workers[10] used ion channeling and infrared absorption spectroscopy analyses to characterize Ge wafers implanted with $^{12}C^+$ and $^{13}C^+$ ions at energies and doses chosen to provide a uniformly doped 0.7-μm-thick region with $y=0.007$. They observed a Ge–C stretch mode at a frequency of 531 cm^{-1}, consistent with predicted values obtained from *ab initio* local density functional cluster theory calculations of the vibrational mode frequencies of substitutional C in Ge, between 516 and 563 cm^{-1}.[10] Analyses of channeling rocking curves around the $\langle 100\rangle$, $\langle 110\rangle$, and $\langle 111\rangle$ axes suggested that up to 31%±3% of the incorporated C was in substitutional sites.

Todd *et al.*[11] reported the growth of $Ge_{1-y}C_y$ ($y=0.015-0.05$) on Si(001) by ultrahigh-vacuum CVD, but provided no evidence for substitutional C and did not address the strain state of the layers. XRD studies of MBE $Ge_{1-y}C_y/Si(001)$ layers grown at $T_s=600\,^\circ C$ with $y=0.01-0.03$[12] revealed a weak forbidden 002 peak which suggests that some C may have been incorporated into substitutional sites. However, the relaxed lattice constant determined from XRD analyses of a $Ge_{0.97}C_{0.03}$ sample was 5.6525 Å, much larger than the 5.5940 Å value predicted using Vegard's rule. This indicates that either there is only a very small fraction ($y<0.0024$) of incorporated C atoms on-site, and/or that part of the strain due to the substitutional C is compensated by the presence of C in other sites such as interstitials.

Lowering the growth temperature to $T_s=200\,^\circ C$ during $Ge_{1-y}C_y/Si(001)$ MBE with $y\leqslant 0.1$ (Ref. 13) still only resulted in a maximum substitutional C fraction of $\simeq 0.01$ as determined from XRD, while Raman spectroscopy showed evidence of amorphous C (presumably at the surface and decorating extended defects) in films with $y\geqslant 0.02$. The authors proposed that for growth conditions leading to a C content exceeding the total solubility limit for both substitutional and interstitial C, an amorphous C layer forms on the surface, causing the growth front to become three dimensional. With continued deposition, island coalescence produces extended defects. The use of Sn as a surfactant during solid-source MBE $Ge_{1-y}C_y$ on Si(001) at $T_s=500\,^\circ C$ was shown to inhibit Stranski–Krastanov islanding, but did not increase the C concentration incorporated into substitutional sites above $y=0.01$.[14]

There are essentially no data for $Ge_{1-y}C_y$ growth on Ge(001). Yang *et al.*[13] noted that $Ge_{0.95}C_{0.05}$ grows epitaxially on Ge(001) but yields highly defective layers with rough 113 faceted surfaces. The Raman local vibrational mode for substitutional C in Ge was identified as a narrow line at 530 cm^{-1},[15] consistent with the data of Hoffman *et al.*[10]

In this article, we present initial results on the use of hyperthermal beams to grow metastable $Ge_{1-y}C_y$($y\leqslant 0.02$) alloys on Ge(001). We find that the C atoms are incorporated into one or more of three sites in the Ge crystal—substitutional, interstitial, and extended defects—with the distribution depending upon T_s which was varied between 200 and 550 °C. All alloys, irrespective of T_s, are fully coherent with the substrate as judged by high-resolution x-ray reciprocal lattice mapping (HR-RLM) and cross-section transmission electron microscopy (XTEM) analyses. Films grown at $T_s\geqslant 450\,^\circ C$ are nearly strain free due to C incorporation into extended defects, whereas alloys deposited at lower temperature are in compression due to the concentration of C incorporated into nonsubstitutional sites exceeding that in substitutional sites. High-resolution XRD diffraction (HR-XRD) and HR-RLM results clearly demonstrate that nonsubstitutional C atoms induce large compressive strain, which cannot be neglected when determining the total incorporated C fraction from diffraction analyses. Vacuum annealing films grown at $T_s\leqslant 350\,^\circ C$ at temperatures up to $T_a=550\,^\circ C$ increases the in-plane compressive strain, whereas the formation of dislocation loops, acting as sinks for C, occurs after annealing at $T_a=650\,^\circ C$, thus relieving the strain in the films. The strain in alloys grown at $T_s\geqslant 450\,^\circ C$ remains unchanged during annealing since all C is already incorporated in extended defects.

II. EXPERIMENTAL PROCEDURE

All film growth experiments were conducted in an ultrahigh-vacuum (UHV) three-chamber load-locked stainless-steel system. The growth chamber is cryopumped with a base pressure of 1×10^{-10} Torr and contains facilities for *in situ* reflection high-energy electron-diffraction and residual gas analysis while the ion-pumped analytical chamber is equipped with an Auger electron spectroscopy system.[16] In the present experiments, 1 keV Kr^+ ions were used to sputter

undoped float-zone Ge and high-purity C targets in order to generate hyperthermal Ge and C beams. Sputtering is carried out using modified UHV Kaufman-type double-grid multi-aperture broad ion-beam sources with provisions for *in situ* spatial adjustment. Electrodischarge-machined ultrahigh-purity single crystal Si wafers were used as beam-shaping apertures. A detailed discussion of the design, construction, and operation of the ion sources is presented elsewhere.[17]

The Ge and C targets are suspended on an insulating cantilever and can be adjusted with respect to the substrate to exploit the angular distribution of reflected neutral particles and to optimize film-thickness uniformity. The ion beam is focused by a postextraction unipotential electrostatic lens, which also acts as a mirror to prevent electron backstreaming from the neutralization device. Space-charge spreading of the ion beam is suppressed immediately upon emerging from the final lens aperture by electron injection from a circular thermionic W filament. The filament is positioned external to the beam in order to eliminate W contamination.

$Ge_{1-y}C_y$ film compositions were controlled through the choice of beam currents from each ion gun. The use of the higher-mass Kr instead of Ar, together with the system geometry described in Ref. 17, minimizes the flux of energetic backscattered particles. The chamber pressure during deposition was 1.2×10^{-4} Torr. TRIM Monte Carlo simulations[18] showed that the energy distribution of the sputtered species has a maximum at 4 eV for Ge and 8 eV for C with average energies of 18 and 24 eV, respectively.

The substrates were polished 1.5×1.5 cm^2 *n*-type Ge(001) wafers with room-temperature resistivities of 1–20 Ω cm ($n=1\times10^{15}$–6×10^{13} cm^{-3}). Substrate cleaning consisted of ultrasonic degreasing, rinsing in de-ionized water to remove the native oxide, and oxidation by a UV–ozone process.[19] The wafers are then bonded to the substrate platen with In and immediately inserted into the UHV system. Final substrate preparation consists of degassing at 200 °C for 30 min followed by desorption of the oxide layer at 450 °C for 60 min. 1000-Å-thick Ge(001) buffer layers were then deposited at $T_s=400$ °C using a growth rate R_{Ge} of 1.4 Å s^{-1}. The $Ge_{1-y}C_y$ alloy layers were grown at $T_s=200$–550 °C with R_{Ge} maintained at 1.4 Å s^{-1}.

$Ge_{1-y}C_y$ film compositions were determined by elastic recoil detection time-of-flight spectroscopy (ERD-TOF)[20] and secondary ion mass spectrometry (SIMS). ERD-TOF elemental depth profiles were obtained using a 30 MeV $^{35}Cl^{5+}$ beam incident at 75° from the surface normal and detecting recoils and scattered ions at 30° with respect to the beam. The energy loss parameters required for analyzing the data were obtained from TRIM 95[18] simulations. SIMS measurements were carried out in a Cameca IMS-5 instrument operated with a 10 kV Cs^+ primary ion beam. The Cs^+ current was 30 nA, yielding a sample sputtering rate of $\simeq$5.5 Å s^{-1} as determined by XTEM. ERD-TOF results showed that C concentrations in the alloys increased linearly with the Kr^+ ion beam current at the C target. A small amount of Si, 1.0%±0.2%, independent of the C concentration, was also detected in alloys and buffer layers due to sputtering from the edges of the Si(001) beam-shaping apertures.

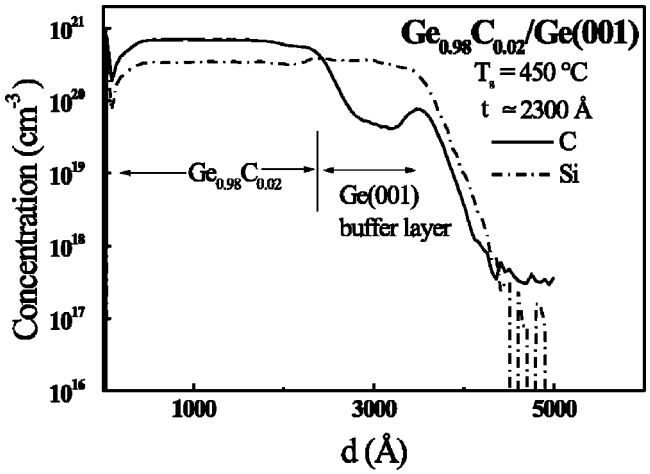

FIG. 1. SIMS depth profiles through a 2300-Å-thick $Ge_{0.99}C_{0.02}$ layer grown at $T_s=450$ °C on a 1150-Å-thick Ge(001) buffer layer. The approximate interface positions are labeled. 1 at. % Si is present in both the buffer and alloy layers.

The microstructure, strain-state, and crystalline quality of the layers were investigated using HR-XRD, HR-RLM, and XTEM. The HR-XRD measurements were performed using a Philips diffractometer with Cu $K_{\alpha1}$ radiation ($\lambda=1.540\,597$ Å) from a four-crystal Ge(220) monochromator which provided an angular divergence of $\simeq$12 arc s with a wavelength spread $\Delta\lambda/\lambda\simeq7\times10^{-5}$. $\omega-2\theta$ overview scans (ω is the x-ray angle of incidence and θ is the Bragg diffraction angle) were obtained with a detector acceptance angle of $\simeq2°$. An additional two-crystal Ge(220) analyzer was placed between the sample and the detector to obtain high-resolution scans (detector acceptance angle $\simeq$12 arc s) and reciprocal lattice maps about both symmetric and asymmetric reflections. The maps are generated by taking repetitive $\omega-2\theta$ scans starting at different initial values of ω.

XTEM examinations were carried out using a Philips CM12 microscope operated at 120 kV. Specimens for XTEM examinations were prepared by gluing two samples film-to-film and then cutting a vertical section which was thinned by mechanical grinding to a thickness of $\simeq25$ μm. Final thinning to electron transparency was done by Ar^+ ion milling in a liquid-N_2-cooled stage in which the incident beam angle and energy were progressively reduced from 15° to 11° and 5 to 3.5 kV in order to minimize radiation damaged artifacts and to obtain samples with relatively uniform thickness distributions.

Postdeposition annealing was performed in a high vacuum chamber. The samples were attached to a W holder and placed in a graphite crucible. Annealing temperatures T_a were measured using a thermocouple. As-deposited $Ge_{1-y}C_y$ alloys were successively annealed at temperatures T_a of 450, 550, and 650 °C for 30 min each.

III. RESULTS

$Ge_{1-y}C_y$ layers with nominal thicknesses *t* of 2300 Å and concentrations $y\leqslant0.02$ were grown at $200\leqslant T_s\leqslant550$ °C. SIMS analyses were performed on all films. A typical depth profile, in this case from a $Ge_{0.98}C_{0.02}$ layer

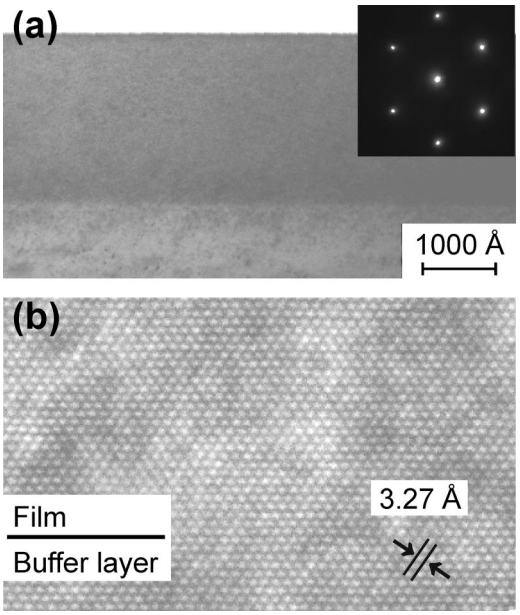

FIG. 2. (a) A bright-field XTEM image, obtained with $\bar{g}=004$ near [110], from a fully strained 2300-Å-thick epitaxial $Ge_{0.99}C_{0.01}$ alloy film grown on Ge(001) at $T_s=300\,°C$. A 110 SAED pattern is shown in the inset. (b) A 110 HR-TEM image of the film shown in (a).

grown at $T_s=450\,°C$, is shown in Fig. 1. C concentrations were found by both SIMS and ERD-TOF analyses to be constant as a function of depth in all layers. The profile in Fig. 1 also reveals the presence of $\simeq 0.1$ at. % C in the buffer layer, as well as 1 at. % Si in both the alloy and buffer layers. The sudden increase in the C signal at a depth d near 3400 Å derives from the extreme sensitivity of C to matrix effects resulting from a small residual oxygen contamination at the substrate/buffer-layer interface.

A combination of HR-XRD, RLM, and XTEM analyses show that all $Ge_{1-y}C_y$ layers are fully coherent with the Ge(001) substrate. Figure 2(a) is a bright field XTEM image, obtained using the diffraction vector $\bar{g}=004$ near the 110 zone axis, from a highly perfect fully strained (as determined by HR-XRD and HR-RLM) $Ge_{0.99}C_{0.01}$ layer grown at $T_s=300\,°C$. The film contains no extended defects, and its surface is flat to within the resolution of TEM. Strain contrast due to lattice constant mismatch is observed at the film/buffer-layer interface. The [110] zone axis selected-area electron-diffraction (SAED) pattern in the inset consists of single-crystal reflections with symmetric intensities. The HR-TEM image in Fig. 2(b) shows 111 lattice fringes which are continuous across the film/buffer-layer interface with no indication of disorder.

$Ge_{1-y}C_y$ alloys grown at $T_s \geqslant 350\,°C$ contain $>1\times10^{13}\ cm^{-3}$ $\langle 111\rangle$ stacking faults and exhibit rough faceted surfaces. Figure 3 is a typical bright-field XTEM image, obtained using $\bar{g}=220$ near the 110 zone axis, from a fully strained 2300-Å-thick $Ge_{0.98}C_{0.02}$ layer grown at $T_s=450\,°C$. The film/buffer-layer interface is abrupt and no misfit dislocations were observed. The peak-to-valley roughness is $\simeq 500$ Å and the angle between [001] and a vector orthogonal to the facet surface is 25.2°. This is in agreement

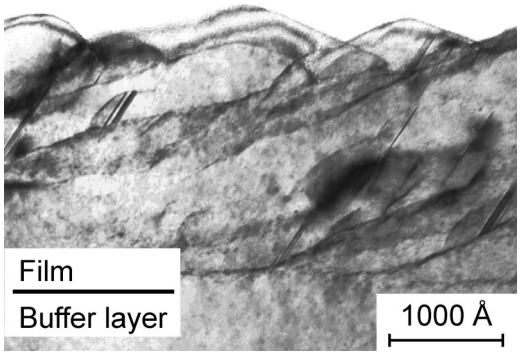

FIG. 3. A bright-field XTEM image, obtained with $\bar{g}=220$ near [110], from a fully strained 2300-Å-thick epitaxial $Ge_{0.98}C_{0.02}$ alloy film grown on Ge(001) at $T_s=450\,°C$.

with analyses of atomic force microscopy images indicating that the facets are terminated by {113} planes.

Typical HR-XRD $\omega-2\theta$ scans through the Ge substrate 004 Bragg peak are presented in Fig. 4 for $Ge_{1-y}C_y$ layers with $y=0.01$ and 0.02 grown at $T_s=200$, 300, 450, and 550 °C. In all cases, the full-width at half-maximum intensity $\Gamma_{\omega-2\theta}$ of the 004 substrate peak is comparable to the theoretical value, 8 arc s. $Ge_{1-y}C_y$ layers grown at $T_s \leqslant 350\,°C$ are in compression with an in-plane strain which decreases with increasing T_s. Films grown at $T_s \geqslant 450\,°C$ are in a weak, but constant, state of tension, irrespective of C content. The layer peak in the $\omega-2\theta$ curve from the $Ge_{0.99}C_{0.01}$ alloy grown at $T_s=550\,°C$ [Fig. 4(a)] occurs on the high-angle side of the substrate peak. The angular separation be-

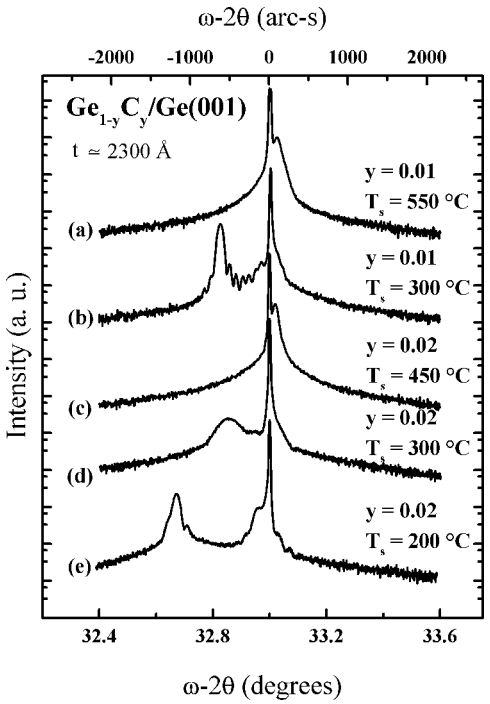

FIG. 4. HR-XRD $\omega-2\theta$ scans around the 004 Bragg peaks from nominally 2300-Å-thick $Ge_{1-y}C_y$ alloys grown on Ge(001): (a) $y=0.01$, $T_s=550\,°C$, (b) $y=0.01$, $T_s=300\,°C$, (c) $y=0.02$, $T_s=450\,°C$, (d) $y=0.02$, $T_s=300\,°C$, and (e) $y=0.02$, $T_s=200\,°C$. Curves are shifted vertically for clarity.

tween the substrate and layer peaks, $\Delta\omega = 98$ arc s, indicates in-plane tension with an out-of-plane lattice constant $a_\perp = 5.654$ Å.

Using the fact that all films are fully strained (see below), we find that the orthogonal and in-plane strains of the film corresponding to Fig. 4(a) are $\varepsilon_\perp = -2.71\times10^{-4}$ and $\varepsilon_\parallel = 3.71\times10^{-4}$, respectively, where $\varepsilon_\perp$ and $\varepsilon_\parallel$ are defined as $\varepsilon_\perp = (a_\perp - a_r)/a_r$ and $\varepsilon_\parallel = (a_\parallel - a_r)/a_r$. a_r is the relaxed alloy lattice constant, obtained using the Ge Poisson ratio. $a_\perp$ for the alloy is equal to the out-of-plane lattice constant expected for a perfectly coherent $Si_{0.01}Ge_{0.99}$ layer on Ge(001), $a_0 = 5.654$ Å. Thus, the incorporated C has a negligible influence on the strain state of the film under these growth conditions. $\Gamma_{\omega-2\theta}$ for the layer peak is 85 arc s. This value is slightly larger than the theoretical minimum value, 73 arc s, obtained from fully dynamical calculations[21,22] due to the presence of extended defects in the film as observed by XTEM. $Ge_{0.99}C_{0.01}$ layers grown at $T_s = 450\,^\circ$C (not shown) were also found to be in tension with an out-of-plane lattice constant $a_\perp = 5.654$ Å.

Decreasing T_s while maintaining the C content at 1 at. % results in the appearance of the layer HR-XRD peak position at ω values smaller than the Ge peak position. Films grown at $T_s \leqslant 350\,^\circ$C are in a state of in-plane compression, suggesting that a significant fraction of incorporated C resides on interstitial sites. Figure 4(b) corresponds to a $Ge_{0.99}C_{0.01}$ film grown at $T_s = 300\,^\circ$C. The film is coherent with the Ge(001) substrate (from HR-RLM results) with $a_\perp = 5.684$ Å ($\varepsilon_\perp = 1.97\times10^{-3}$, $\varepsilon_\parallel = -2.68\times10^{-3}$). Finite-thickness interference fringes are clearly visible, indicating excellent film crystalline quality and a laterally uniformly flat buffer-layer/film interface. From the fringe spacing, we calculate a film thickness of 2365 Å, close to the nominal value of 2300 Å.

The same general trend with respect to film growth temperature is observed for $Ge_{0.98}C_{0.02}$ alloys [Figs. 4(c)–4(e)]. Layers grown at $T_s \geqslant 450\,^\circ$C, are fully strained and slightly in tension with $a_\perp = 5.655$ Å ($\varepsilon_\perp = -1.94\times10^{-4}$, $\varepsilon_\parallel = 2.65\times10^{-4}$), very close to the value expected for a $Si_{0.01}Ge_{0.99}$ alloy grown on Ge(001). The HR-XRD curve for the sample grown at $T_s = 450\,^\circ$C [Fig. 4(c)] exhibits a layer peak with a $\Gamma_{\omega-2\theta}$ value of 80 arc s. $Ge_{0.98}C_{0.02}$ layers grown at $T_s \leqslant 350\,^\circ$C are also coherent but in a state of in-plane compression. For $Ge_{0.98}C_{0.02}$ layers grown at $T_s = 300\,^\circ$C [Fig. 4(d)], the measured out-of-plane lattice constant is 5.678 Å ($\varepsilon_\perp = 1.53\times10^{-3}$, $\varepsilon_\parallel = -2.06\times10^{-3}$). A comparison between the HR-XRD scans in Figs. 4(b) and 4(d) from layers grown at the same temperature ($T_s = 300\,^\circ$C) clearly shows that the crystalline quality decreases as the C content increases. This is attested to by the disappearance of the thickness fringes, the decrease in diffracted intensity, and the increase in $\Gamma_{\omega-2\theta}$.

A further decrease in T_s to 200 °C yields even higher in-plane compression as shown in Fig. 4(e), a HR-XRD scan from a $Ge_{0.98}C_{0.02}$ layer with $a_\perp = 5.708$ Å ($\varepsilon_\perp = 3.76\times10^{-3}$, $\varepsilon_\parallel = -5.10\times10^{-3}$). However, finite-thickness interference fringes are visible near the substrate and layer peaks, indicating that the overall crystallinity of the layer and the flatness of the buffer-layer/alloy-layer interface are higher than for the $Ge_{0.98}C_{0.08}$ layer grown at $T_s = 300\,^\circ$C [Fig. 4(d)].

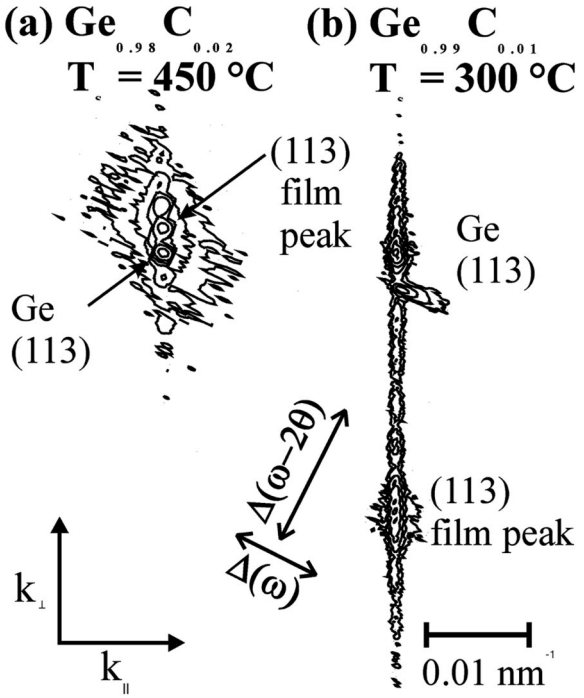

FIG. 5. HR-RLMs around the 113 Bragg peaks from nominally 2300-Å-thick $Ge_{1-y}C_y$ alloys deposited on Ge(001): (a) $y = 0.02$, $T_s = 450\,^\circ$C and (b) $y = 0.01$, $T_s = 300\,^\circ$C. Successive isointensity contours correspond to 4000, 1000, 250, 60, 15, and 4 counts s^{-1}.

The effects of C concentration and film growth temperature on x-ray scattering distributions near the asymmetric 113 Bragg peak with incidence angle $\omega = 1.625\,^\circ$ are illustrated in Fig. 5 showing typical HR-RLMs. Diffracted intensities are plotted as isointensity contours as a function of the reciprocal lattice vectors $k_{||}$ parallel and $k_\perp$ perpendicular to the surface. The layer peak appears above (below) the Ge substrate peak for alloy films in tension (compression). For all films in this investigation, irrespective of C concentration or growth temperature, the layer scattering distributions are perfectly aligned with the substrate scattering distributions in the $k_{||}$ direction as judged by both HR-RLM and HR-XRD using asymmetric complementary reflections. This indicates that all films are fully strained with negligible in-plane strain relaxation to within the detection limit of the instrument, $\simeq 1\times10^{-5}$.

The diffraction contours obtained from the $Ge_{0.98}C_{0.02}$ layers grown at $T_s = 450\,^\circ$C and $T_s = 300\,^\circ$C in Figs. 5(a) and 5(b), respectively, are nearly symmetric except for the elongation in the growth direction due to finite thickness effects. The alloy grown at $T_s = 450\,^\circ$C [Fig. 5(a)] also shows a slight broadening in the ω direction at low counts. Γ_ω and $\Gamma_{\omega-2\theta}$ are 37 and 18 arc s, respectively. The position of the layer peak with respect to that of the substrate yields $a_\perp = 5.654$ Å and Γ_ω is larger than the theoretical value, 17 arc s, indicative of sample mosaicity. The broadening of the peak in the low count regions in the ω direction suggests a nonmicroscopically abrupt interface, consistent with the dis-

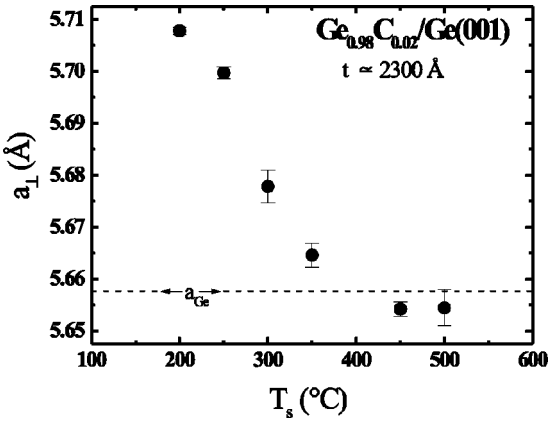

FIG. 6. Lattice parameter $a_\perp$ along the film growth direction vs the growth temperature T_s for a series of nominally 2300-Å-thick $Ge_{0.98}C_{0.02}$ layers grown on Ge(001).

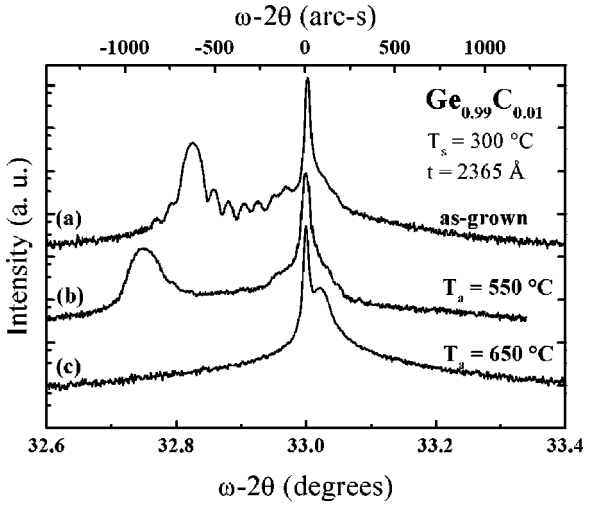

FIG. 7. HR-XRD $\omega-2\theta$ scans around the 004 Bragg peaks from (a) an as-deposited 2365-Å-thick $Ge_{0.99}C_{0.01}$ alloy grown at $T_s=300\,^\circ$C and (b) after annealing for 30 min at $T_a=550\,^\circ$C, and (c) after further annealing for 30 min at $T_a=650\,^\circ$C. Curves are shifted vertically for clarity.

appearance of thickness fringes as also observed in the HR-XRD pattern [Fig. 4(c)].

Γ_ω and $\Gamma_{\omega-2\theta}$ values for the $Ge_{0.99}C_{0.01}$ layer grown at $T_s=300\,^\circ$C [Fig. 5(b)] are 17 and 16 arc s, respectively, nearly equal to the corresponding values for the substrate diffraction distributions, 17 and 14 arc s. Finite thickness interference fringes are clearly visible as periodic intensity contours positioned along $k_\perp$. The vertical separation between the film and the substrate diffracted intensity distributions in Fig. 5(b) corresponds to a tetragonal distortion in the growth direction of $\varepsilon_\perp=1.8\times10^{-3}$, yielding $a_\perp=5.681$ Å, in good agreement with the HR-XRD results. The diffraction distributions observed just below the substrate peak are attributed to the 1000-Å-thick Ge buffer layer which contains $\leqslant$0.1 at. % C. The contours for this peak are slightly elongated in the ω and $k_\parallel$ directions due to the small residual contamination at the substrate/buffer-layer interface visible by XTEM and in SIMS depth profiles. The buffer layer buries the residual contamination and provides a highly perfect initial template, as shown in the HR-TEM image in Fig. 2(b), for the growth of $Ge_{1-y}C_y$ alloy overlayers.

$Ge_{0.98}C_{0.02}$ lattice constants $a_\perp$ along the growth direction are plotted in Fig. 6 as a function of T_s. Two regimes are clearly visible. Over the growth temperature range $T_s=200-350\,^\circ$C, $a_\perp$ is greater than a_{Ge} (indicating in-plane compression) and decreases continuously from 5.708 to 5.664 Å with increasing T_s. For growth temperatures $T_s\geqslant450\,^\circ$C, $a_\perp$ is less than a_{Ge} and approximately equal to the lattice constant of a coherent $Si_{0.01}Ge_{0.99}$ layer grown on Ge(001).

The fact that the films grown at T_s less or equal to 350 °C exhibit in-plane compression, $-5.10\times10^{-3}\leqslant\varepsilon_\parallel\leqslant-2.17\times10^{-3}$, suggests that a significant fraction of the incorporated C resides in interstitial sites since substitutional C gives rise to in-plane tension. Arguing in analogy with previous results for the $Si_{1-x}C_x$ system,[9] the configuration is likely to be a Ge–C split interstitial. $Ge_{1-y}C_y$ alloys grown at $T_s\geqslant450\,^\circ$C exhibit a macroscopic in-plane tensile strain, $\varepsilon_\parallel=3.71\times10^{-4}$, which is much smaller than the expected value if all C resided on Ge substitutional sites. Assuming Vegard's rule yields $\varepsilon_\parallel=7.45\times10^{-3}$, approximately 20 times larger than the experimental value. The small tensile strain in the $T_s\geqslant450\,^\circ$C layers can be explained by the unintentional incorporation of $\simeq1$ at. % Si, with the incorporated C making no contribution to the net strain.

Annealing experiments were carried out to study the thermal stability of as-deposited $Ge_{1-y}C_y$ alloy layers. All samples were successively annealed at $T_a=450$, 550, and 650 °C for 30 min each and changes in the lattice constants were determined at each step by HR-XRD. SIMS depth profiles after annealing were identical to those obtained from as-deposited samples.

Figure 7 compares HR-XRD $\omega-2\theta$ scans from an as-deposited 2365-Å-thick $Ge_{0.99}C_{0.01}$ alloy grown at $T_s=300\,^\circ$C with those obtained after annealing at $T_a=550$ and 650 °C. The 450 °C anneal (not shown) resulted in the film peak moving to lower ω values, thus increasing the in-plane compressive strain and out-of-plane lattice constant to $\varepsilon_\parallel=-3.28\times10^{-3}$ and $a_\perp=5.690$ Å, respectively. Further annealing at $T_a=550\,^\circ$C [Fig. 7(b)] yielded larger strains, $\varepsilon_\parallel=-3.79\times10^{-3}$ and $a_\perp=5.695$ Å, accompanied by the disappearance of the finite-thickness interference fringes. The

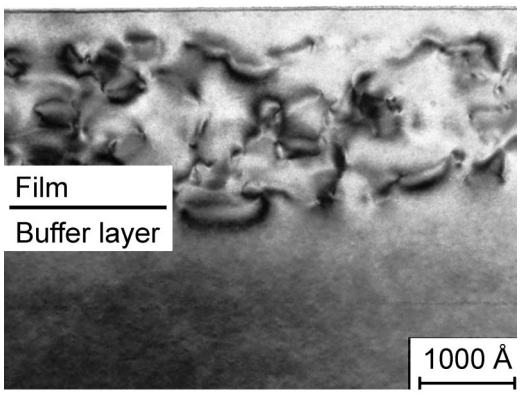

FIG. 8. A bright-field XTEM image, obtained with $\bar{g}=220$ near [110], of the sample corresponding to Fig. 7(c).

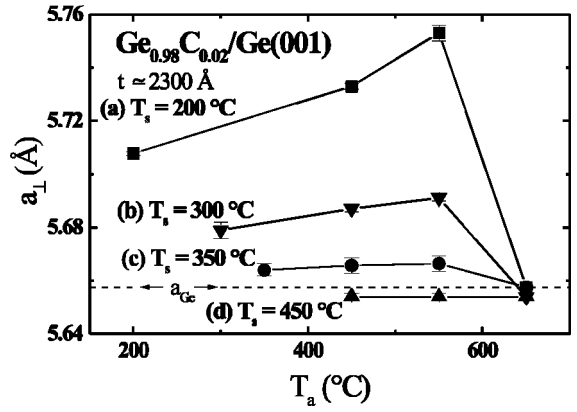

FIG. 9. Lattice parameter $a_\perp$ along the film growth direction as a function of the annealing temperature T_a for nominally 2300-Å-thick $Ge_{0.98}C_{0.02}$ alloys grown on Ge(001) at: (a) $T_s = 200\,^\circ$C, (b) 300 °C, (c) 350 °C, and (d) 450 °C. For each curve, the point at the lowest temperature corresponds to $a_\perp$ for the as-deposited layer.

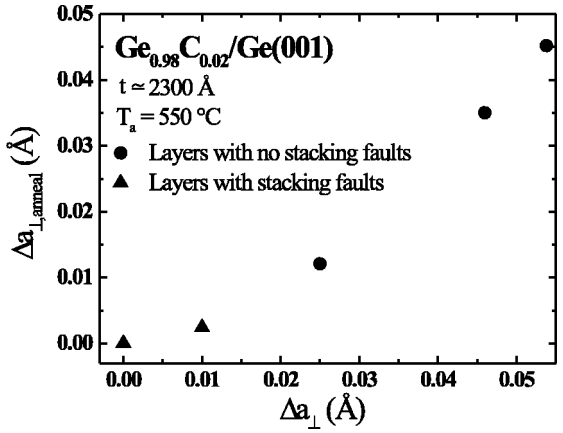

FIG. 10. Variation of $\Delta a_{\perp,\text{anneal}}$ vs $\Delta a_\perp$ for $Ge_{0.98}C_{0.02}$ layers annealed at $T_a = 550\,^\circ$C for 30 min. Circles and triangles correspond to layers with no extended defects and with stacking faults, respectively.

latter indicates a decrease in film crystalline quality, although corresponding high-resolution reciprocal lattice maps show that the film remains coherent with the substrate. Annealing at $T_a = 650\,^\circ$C produced even more dramatic effects. The film peak [Fig. 7(c)] shifted to larger angles, in fact all the way to the right of the substrate peak. Thus, the film is now in tension with an out-of-plane lattice constant, $a_\perp = 5.654$ Å, smaller than a_{Ge}. The lattice constant is now very close to that of as-deposited $Ge_{0.99}C_{0.01}$ layers grown at $T_s \geqslant 450\,^\circ$C.

In situ annealing experiments carried out in the TEM on $Ge_{0.99}C_{0.01}$ alloys grown at $T_s = 300\,^\circ$C reveal no changes in film microstructure until the abrupt appearance of dislocation loops at $T_a \simeq 600\,^\circ$C. The XTEM bright-field image in Fig. 8, obtained under two-beam conditions with the diffraction vector $\bar{g} = 004$, shows a $Ge_{0.99}C_{0.01}$ sample grown at $T_s = 300\,^\circ$C after successive *ex situ* 30 min anneals at 450, 550, and 650 °C. The image is dominated by a high number density of dislocation loops distributed uniformly across the thickness of the alloy layer. However, no dislocations were observed in the buffer layer, the film surface remains smooth, and there were no misfit dislocations at the buffer-layer/film interface. The latter result is consistent with HR-XRD and HR-RLM results showing the film to be coherent with the substrate.

Figure 9 is a plot of $a_\perp$, determined by HR-XRD, as a function of T_a for $Ge_{0.98}C_{0.02}$ layers grown at $T_s = 200-450\,^\circ$C. For each curve, the point at the lowest temperature corresponds to $a_\perp$ for the as-deposited layers. As-deposited films in tension ($T_s \geqslant 450\,^\circ$C) remain unchanged after annealing. However, the results for layers grown at $T_s \leqslant 350\,^\circ$C, which exhibit in-plane compression, follow the general trend observed for $Ge_{0.99}C_{0.01}$ in Fig. 7. $a_\perp$ increases with T_a, until dislocation loops are formed at $T_a \simeq 600\,^\circ$C, thus relieving the strain. The variation in the alloy lattice constant $\Delta a_{\perp,\text{anneal}}$ following a 30 min anneal at 550 °C, is plotted in Fig. 10 versus the initial lattice constant difference, $\Delta a_\perp = (a_\perp - a_0)$, where a_0 is the relaxed lattice constant in the absence of C. For layers with no extended defects, $\Delta a_{\perp,\text{anneal}}$ increases approximately linearly with $\Delta a_\perp$ suggesting, as discussed in Sec. IV, that $\Delta a_{\perp,\text{anneal}}$ is proportional to the initial interstitial C content in the layer.

IV. DISCUSSION

$Ge_{1-y}C_y$ alloys ($y \leqslant 0.02$) grown on Ge(001) at $T_s = 200-550\,^\circ$C from hyperthermal beams are fully coherent as judged by HR-RLM, HR-XRD, and XTEM. The total incorporated C concentrations measured by ERD-TOF and SIMS agree well with values expected from growth rate calibrations and were found to be independent of T_s. $Ge_{0.98}C_{0.02}$ layers grown at low temperatures ($T_s \leqslant 350\,^\circ$C) exhibit compressive in-plane strain which decreases with increasing T_s. Layers grown at $T_s \geqslant 450\,^\circ$C are in a weak state of tension due purely to the unintentional presence of 1 at. % Si. Measured out-of-plane lattice constants in $T_s \geqslant 450\,^\circ$C layers are consistent with the value calculated for pseudomorphically grown $Si_{0.01}Ge_{0.99}$ on Ge(001). This, as discussed below, indicates that C atoms in layers grown at $T_s \geqslant 450\,^\circ$C are incorporated in a strain-free lattice configuration.

This is the first report of in-plane compression in $Ge_{1-y}C_y$ layers grown on Ge(001). We attribute the compression to the hyperthermal-irradiation-induced formation of Ge–C split interstitials during film growth.[23] Molecular dynamics and quasidynamics simulations indicate that interstitials are created by 10 eV, and both interstitials and vacancies are created by 50 eV, hyperthermal Si atoms during Si(001) MBE.[24,25] However, the point defects are annealed out by near-surface recombination and by annihilation at the surface during deposition at normal growth temperatures and rates. This is attested to by the fact that homoepitaxial Si(001):Sb (Ref. 26) and Ge(001):Al (Ref. 17) layers grown at 400–750 and 400–600 °C, respectively, in the same system with similar growth conditions as used here, exhibit carrier mobilities equal or better than reported values for bulk Si and Ge.

During film growth from hyperthermal beams generated by a sputtered source, species incident at the film surface with translational energies in the high-energy tail of the distribution result in the formation of self-interstitials. In the

case of Ge growth at the temperatures used in the present experiments, we expect, based upon the results of Refs. 24 and 25, that essentially all interstitials will be annealed out during deposition. However, for $Ge_{1-y}C_y$, a fraction of the incorporated C atoms react with Ge self-interstitials to form Ge–C split interstitials, which reside on single lattice sites and give rise to compressive strain. A similar reaction was reported in Si during electron irradiation experiments,[27] where substitutional C atoms react with Si self-interstitials to produce the Si–C split interstitials. In our $Ge_{1-y}C_y$ layers with no extended defects, $T_s \leqslant 300\,^{\circ}C$, we find that the concentration of Ge–C split interstitials decreases with increasing T_s indicating more efficient annealing of Ge interstitials and/or thermally induced decomposition of the Ge–C split interstitials. Due to the high formation energy of the Ge interstitials compared to the Ge–C split interstitials, the latter reaction can only happen, with significant probability, near the surface where the Ge self-interstitial is rapidly lost to the surface sink.

Layers grown at $T_s \geqslant 350\,^{\circ}C$ contain stacking faults which act as sinks for C atoms that are incorporated in a macroscopically strain-free lattice configuration. The increasing stacking fault density in films grown at $T_s \geqslant 350\,^{\circ}C$, together with the observed reduction in the overall strain, suggest that the fraction of C incorporated in extended defects sites increases with T_s. HR-XRD and HR-RLM analyses of $T_s \geqslant 450\,^{\circ}C$ layers provide no evidence for the presence of C in either substitutional or split-interstitial configurations. Moreover, C trapping is a synergistic reaction in the sense that the stacking fault formation energy is reduced by the presence of C atoms as demonstrated by Ge homoepitaxy experiments, where Ge(001) layers grown in the same system under similar conditions are highly perfect single crystals.[17]

The results presented above indicate that C can be incorporated into at least three different lattice configurations: substitutional, interstitial, and at extended defects sites. While measurements of y and $a_\perp$ provide important insights into the relative concentrations of the three different C configurations as a function of T_s, absolute concentration determinations for each configuration are not possible since the strain coefficient for Ge–C split interstitial is unknown. Additional experiments with the ability to directly probe specific C configurations, for example by local vibrational mode measurements, are required in order to extract quantitative site concentration fractions.

Figures 9 and 10 show that the lattice constant along the growth direction $a_\perp$ increases during 450 and 550 °C anneals of $Ge_{1-y}C_y$ layers in compression ($T_s \leqslant 350\,^{\circ}C$). The magnitude of this increase, $\Delta a_{\perp,\mathrm{anneal}}$, is proportional to the dilatation in the as-deposited layers, $\Delta a_\perp = (a_\perp - a_0)$, which is, in turn, proportional to the Ge–C split-interstitial concentration. This suggests that a new C-containing defect complex, with a higher strain coefficient, is generated during postdeposition annealing and that Ge–C split interstitials in the as-deposited layer participate in the formation reaction. A likely possibility is the capture of a bulk thermally produced Ge self-interstitial by a resident Ge–C split interstitial, as reported during electron irradiation of C-doped Si.[28]

During annealing of the tensile-strained layers ($T_s \geqslant 450\,^{\circ}C$), in contrast to the compressive layers, the lattice constant in the growth direction $a_\perp$ remains constant. Thus, C atoms incorporated in extended defects are thermally stable to annealing at temperatures up to at least $T_a = 550\,^{\circ}C$.

Finally, we note that while it is commonly accepted that substitutional and nonsubstitutional C have opposite effects on the strain state of $Si_{1-y}C_y$ and $Ge_{1-y}C_y$ heterostructures, the strain induced by nonsubstitutional C is rarely considered in the analyses and the substitutional C fraction is generally extracted from XRD results alone. Our results clearly demonstrate that the strain induced by nonsubstitutional C, especially split interstitials, is significant and must be explicitly accounted for in the quantitative determination of the substitutional C concentrations from HR-XRD analyses.

V. CONCLUSIONS

Epitaxial metastable $Ge_{1-y}C_y/Ge(001)$ alloys with $y \leqslant 0.02$ were grown at $T_s = 200–550\,^{\circ}C$ from hyperthermal Ge and C beams with average energies of 16 and 24 eV, respectively. All films, irrespective of T_s, are fully coherent with the substrate as judged by HR-RLM and XTEM analyses. Three different C configurations were identified in the films: substitutional, Ge–C split interstitials, and C trapped at extended defects. Layers grown at $T_s \leqslant 350\,^{\circ}C$ are in compression due to having higher concentrations of Ge–C split interstitials than substitutional C. The Ge–C split interstitials are formed as a result of the reaction of incorporated C with Ge interstitials created by the hyperthermal-beam irradiation during film growth. The decrease in compressive strain with increasing T_s is due to the more efficient annealing of Ge interstitials during deposition and/or decomposition of Ge–C split interstitials. Postannealing these samples results in the formation of new defect complexes with compressive strain coefficients larger than that of Ge–C split interstitials until, at $T_a \simeq 600\,^{\circ}C$, dislocation loops are nucleated.

Films grown at $T_s \geqslant 350\,^{\circ}C$ contain stacking faults which act as sinks for incorporated C atoms. Films grown at $T_s \geqslant 450\,^{\circ}C$ are macroscopically strain free since all C atoms are located on defect sites. In the intermediate regime, $T_s = 350\,^{\circ}C$, all three configurations—substitutional, Ge–C split interstitial, and extended defects trap sites—coexist. Finally, HR-XRD and HR-RLM results clearly demonstrate that nonsubstitutional C atoms induce large compressive strain which cannot be neglected when determining the total incorporated C fraction from diffraction analyses.

ACKNOWLEDGMENTS

The authors gratefully acknowledge financial support from the Semiconductor Research Corporation and the U.S. Department of Energy Division of Materials Sciences under Contract No. DEFG02-96ER45439. They appreciate the use of the facilities of the Center for Microanalysis of Materials, which is partially supported by DOE, at the University of Illinois. J. D.-G. was partially supported by the Fonds pour la Formation de Chercheurs et l'Aide à la Recherche du Qué-

bec while P. D. and J. D.-G. were partially supported by the Natural Sciences and Engineering Research Council of Canada.

[1] R. A. Soref, J. Appl. Phys. **70**, 2470 (1991).
[2] H. J. Osten, B. Heinemann, D. Knoll, G. Lippert, and H. Rücker, J. Vac. Sci. Technol. B **16**, 1750 (1998).
[3] K. W. Faschinger, S. Zerlauth, G. Bauer, and L. Palmetshofer, Appl. Phys. Lett. **67**, 3933 (1995).
[4] R. I. Scace and G. A. Slack, J. Chem. Phys. **30**, 1551 (1959).
[5] J. Tersoff, Phys. Rev. Lett. **74**, 5080 (1995).
[6] See, for example, H. J. Osten, J. Griesche, and S. Scalese, Appl. Phys. Lett. **74**, 836 (1999); J. L. Hoyt, T. O. Mitchell, K. Rim, D. V. Singh, and J. F. Gibbons, Thin Solid Films **321**, 41 (1998).
[7] T. Laursen, D. Chandrasekhar, David J. Smith, E. T. Croke, and A. T. Hunter, Thin Solid Films **308–309**, 358 (1997).
[8] J. Tersoff, Phys. Rev. Lett. **64**, 1757 (1990).
[9] W. Windl, O. F. Sankey, and J. Menéndez, Phys. Rev. B **57**, 2431 (1998).
[10] L. Hoffman, J. C. Bach, B. Bech Nielsen, P. Leary, R. Jones, and S. Öberg, Phys. Rev. B **55**, 11167 (1997).
[11] M. Todd, J. Kouvetakis, and D. J. Smith, Appl. Phys. Lett. **68**, 2407 (1996).
[12] J. Kolodzey, P. A. O'Neil, S. Zhang, B. A. Orner, K. Roe, K. M. Unruh, C. P. Swann, M. M. Waite, and S. I. Shah, Appl. Phys. Lett. **67**, 1865 (1995).
[13] B.-K. Yang, M. Krishnamurthy, and W. H. Weber, J. Appl. Phys. **82**, 3295 (1997).
[14] H. J. Osten, E. Bugiel, and P. Zaumseil, J. Cryst. Growth **142**, 322 (1994).
[15] W. H. Weber, B.-K. Yang, and M. Krishnamurthy, Appl. Phys. Lett. **73**, 626 (1998).
[16] N.-E. Lee, M. Matsuoka, M. R. Sardela, Jr., F. Tian, and J. E. Greene, J. Appl. Phys. **80**, 812 (1996).
[17] G. A. Tomasch, Y.-M. Kim, L. C. Markert, N.-E. Lee, and J. E. Greene, Thin Solid Films **223**, 212 (1993).
[18] J. F. Ziegler, J. P. Biersack, and U. Littmark, *Stopping and Ranges of Ions in Solids* (Pergamon, New York, 1985).
[19] X.-J. Zhang, G. Xue, A. Agarwal, R. Tsu, M.-A. Hasan, J. E. Greene, and A. Rockett, J. Vac. Sci. Technol. A **11**, 2553 (1993).
[20] S. C. Gujrathi, S. Roorda, J. G. D'Arcy, R. J. Pflueger, P. Desjardins, I. Petrov, and J. E. Greene, Nucl. Instrum. Methods Phys. Res. B **136–138**, 654 (1998).
[21] D. Taupin, Bull. Soc. Fr. Mineral. Crystallogr. **87**, 469 (1964).
[22] S. Tagaki, Acta Crystallogr. **15**, 1311 (1962).
[23] Si–C split interstitials may also form due to the presence of 1 at. % Si, but their concentration is expected to be negligible.
[24] M. Kitabatake, P. Fons, and J. E. Greene, J. Vac. Sci. Technol. A **8**, 3726 (1990).
[25] M. Kitabatake and J. E. Greene, J. Appl. Phys. **73**, 3183 (1993).
[26] N.-E. Lee, G. Xue, and J. E. Greene, J. Appl. Phys. **80**, 769 (1996).
[27] G. Davies and R. C. Newman, in *Handbook on Semiconductors*, edited by S. Mahajan (Elsevier, New York, 1994), Vol. 3, p. 1557.
[28] S. P. Chappell and R. C. Newman, Semicond. Sci. Technol. **2**, 691 (1987).